ChemComm

Superprotonic Conduction through One-dimensional Ordered Alkali Metal Ion Chain in a Lanthanide-Organic Framework

Journal:	*ChemComm*
Manuscript ID	CC-COM-01-2018-000572.R1
Article Type:	Communication

ChemComm

COMMUNICATION

Superprotonic Conduction through One-dimensional Ordered Alkali Metal Ion Chain in a Lanthanide-Organic Framework

Received 00th January 20xx,
Accepted 00th January 20xx

DOI: 10.1039/x0xx00000x

www.rsc.org/

Xia Wang,[a,‡] Yanlong Wang,[a,‡] Mark A. Silver,[a] Daxiang Gui,[a] Zhuanling Bai,[a] Yaxing Wang,[a] Wei liu,[a] Lanhua Chen,[a] Juan Diwu,[a] Zhifang Chai,[a] and Shuao Wang*[a]

Although no evident hydrogen-bond network appears, an ultrahigh proton conductivity of 2.91 × 10^{-2} S cm^{-1} at 363 K and 90% RH with an ultralow activation energy of 0.10 eV was observed in an anionic lanthanide-organic framework $Na_2[Eu(SDB)_2(COO)]·0.375DMF·0.4H_2O$ (1); both values approach the records among all reported proton-conducting MOF materials. This suggests that the proton conduction process in 1 is reminiscent of the Grotthuss mechanism, which together reveals an effective proton transportation pathway associated with aligned Na^+ and their coordinated-water.

Metal-organic frameworks (MOFs) have become ideal candidates for applications of proton conductivity, because of the abilities to tune pore sizes without hindering the chemical stability, uniform architecture, and the feasibility of hybridization with various of materials.[1-18] Due to their well-defined crystalline structures, MOF materials can provide deep insight into proton conduction mechanisms by providing the exact pathway in which the process is carried out. Defining these mechanisms helps to synthesize crystalline materials endowed with higher proton conductivity. To achieving high proton conductivity in MOFs, there are generally three routes: building of materials with ordered hydrogen bond network,[8,19] isomorphous ligand replacement of the framework to introduce acidic functional groups such as carboxyl or sulfonate,[20] incorporation of proton-carriers within the pores (e.g. phosphoric acid).[21-23]

Alkali metal ion and alkali-water clusters have been intensively investigated in many fields owing to the importance of ion-water interactions in a variety of chemical and biochemical phenomena.[24,25] In general, the process of proton transportation predominantly occurs by water molecules playing a pivotal role, not only by forming hydrogen-bonding network within the framework, but acting as proton carriers.[1-3] Owing to the strong interactions between alkali cations and water, alkali-based MOFs show a lot of advantages in proton conduction. For instance, Demadis and co-workers have reported a series of alkali metal phosphonocarboxylates via reactions of a multitude of alkali metal ions with racemic R,S-hydroxyphosphonoacetate (M-HPAA; M = Li, Na, K, Cs). Because this series possesses frameworks with different dimensions, they exhibit a range of proton conductivity from 3.5 × 10^{-5} to 5.6 × 10^{-3} S cm^{-1} at 24 °C and 98% relative humidity (RH).[26] However, researches regarding proton conduction in anionic MOFs whose channels contain alkali ions are extremely rare, and the function of these cations during proton conduction remains unclear.

Herein, we introduce a new 2D anionic MOF with Na^+ orderly arranged in channels, $Na_2[Eu(SDB)_2(COO)]·0.375DMF·0.4H_2O$ (denoted as **1,** H_2SDB = 4,4'-sulfonyldibenzoic acid). The synthesis of **1** was optimized by utilizing a solvothermal reaction of $Eu(NO_3)_3·6H_2O$ and H_2SDB in a mixture of DMF and H_2O. Remarkably, **1** shows high proton conductivity (2.91 × 10^{-2} S cm^{-1} at 363 K and 90% RH) with an ultralow activation energy (0.10 eV). Proton conduction experiments were also carried out with **1** exchanged with Li^+, and the significant change in proton conductivity and activation energy confirms the key role that ordered Na^+ plays in proton transportation.

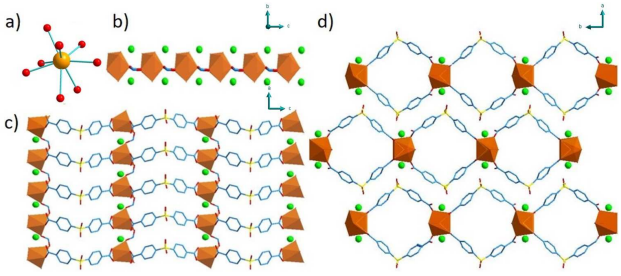

Figure 1. a) The coordination environment of Eu^{3+} center. b) The metal-formate chains with ordered Na^+. c) The layer connected by ligands; d)The layered structure with Na^+ arrange orderly in channels. Color code: Eu in orange, Na in green, O in red, C in blue, and S in yellow. All hydrogen atoms have been removed for clarity.

Single crystal X-ray diffraction analysis reveals that **1** crystallizes in the orthorhombic space group, *Pnma*. As shown in **Fig. S1**, the asymmetric unit of **1** consists of one half of the Eu^{3+} ion and formate, one SDB^{2-} as well as one Na^+ ion. The Eu^{3+} metal centre is

[a] State Key Laboratory of Radiation Medicine and Protection, School for Radiological and interdisciplinary Sciences (RAD-X) and Collaborative Innovation Center of Radiation Medicine of Jiangsu Higher Education Institutions, Soochow University, Suzhou 215123, China. *E-mail:* shuaowang@suda.edu.cn
‡ These authors contributed equally.
Electronic Supplementary Information (ESI) available: [Experimental methods, Details of synthesis, The crystal data, The diagrams of asymmetric unit, EDS data, The diagrams of impedance spectrum]. See
DOI: 10.1039/x0xx00000x

eight-coordinate, whereby six oxygen atoms are donated from four SDB ligands and two are from two formate groups. This means that one C=O group is left free from coordinating Eu^{3+} and instead help to establish an ordered series of Na^{+} down the *c*-axis. Formate ligands link adjacent europium distorted square antiprisms to propagate a metal-organic chain down the *c*-axis. SDB^{2-} ligands bend into a V-shaped linker to connect these 1D-chains to form layers between which 1D rhombus channels are observed. It is within these channels that Na^{+} cations reside. The Na^{+} cations are surrounded by six oxygen atoms from carboxylate, formate, and one of the S=O group to further form a pseudo-3D structure. The distance between adjacent Na^{+} cations is 5.7141(5) Å, which is too far to achieve ionic conduction. The distance between two adjacent oxygen atoms from one O=S=O of ligand is 2.4904(2) Å which is suitable for forming a hydrogen bond; however no residual density indicative of a hydrogen bound to these oxygen atoms was located. The distance between two oxygen atoms from adjacent O=S=O groups is 3.4853(3) Å. Not only are S=O groups terminal in **1**, but C=O groups from SDB ligands accent the porous channels, a distance between two adjacent oxygen atoms is 5.7141(5) Å. This distance is identical to that of Na^{+} described above, supporting the strong interactions between these two species.

Powder X-ray diffraction (PXRD) analysis reveals the phase purity of **1**. Thermal gravimetric analysis was performed to confirm the thermal stability of **1**. As shown in **Fig. 2a**, approx. 0.8% weight loss occurs before 100 °C and is indicative of the loss of 0.4 H_2O. A second weight loss up to 285 °C of approx. 3.1% has been attributed to the loss of DMF. Beyond this, collapse of the framework occurs in steps up to the final temperature of 900 °C. Taking into consideration of the strong interaction between Na^{+} and water in the structure, water vapor adsorption in **1** was measured at different RH. **1** exhibits a moderate water vapor adsorption ability of ca. 110 $cm^3\ g^{-1}$ (**Fig. 3**), despite possessing a relatively high porosity of 62.29% (ca. with PLATON[27]). In addition, from the low angle peaks in the PXRD patterns taken under different RH (from 40% RH to 90% RH), a water induced shrinking of layer spacing was observed (**Fig. S4, S5 and S6**). It is most plausible that adsorbing water molecules would prefer to reside in a thermodynamically favorable position within **1**. A further inspection on the coordination geometry of Na^{+} yields a highly distorted octahedron geometry with considerable amount of room to locate an adsorbed water molecule (**Fig. S13**). From our structural analysis, open pores provide access to terminal oxygen atoms (i.e. C=O, S=O) and ordered Na^{+} in close enough proximity to yield sites capable of producing strong interactions with water molecules. The newly formed hydrogen bond is consistent with the shrink of layer spacing (**Fig. S7**). In addition, the existence of highly mobile protons in the system can be confirmed by the ^{1}H double-quantum (DQ)-filtered solid-state NMR spectrum (**Fig. S8**).[28]

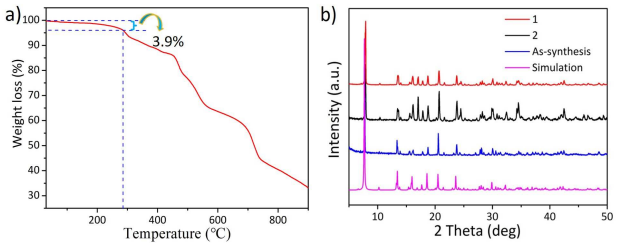

Figure 2. a) TGA of **1** from 0 to 900 °C. b) PXRD of **1** after water vapor adsorption (1, red), after proton conduction (2, black), as-synthesized (blue), and simulation (pink).

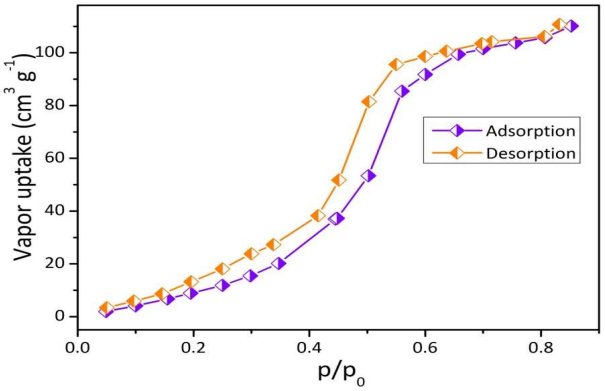

Figure 3. Water vapor adsorption in **1**.

The proton conductivity of **1** was measured under various temperature, humidity, and electrochemical conditions. The conductivity of a thin pellet sample **1** was measured at 303 K and 40% and 60% RH to be 8.67×10^{-5} S cm^{-1} and 4.34×10^{-4} S cm^{-1} (**Fig. 4d**), respectively. Further humidification of **1** is accompanied by a higher proton conductivity of 8.78×10^{-3} S cm^{-1} at 303 K and 90% RH (**Fig. 4b**). Increasing the temperature of the measurement to 363 K at 90% RH allows **1** to achieve an even higher proton conductivity of 2.91×10^{-2} S cm^{-1} (**Fig. 4a**). This direct relationship between the drastic increase in proton conductivity with the increase in humidity reveals that proton transportation in **1** is associated with water adsorption. Traditional low-temperature proton-conducting materials behave similarly, where water content significantly affects the efficiency of proton transportation. Moving further, the activation energy of **1** was calculated from the temperature-dependent behavior determined from the AC impedance spectra to be 0.10 eV (**Fig. 4c**), one of the lowest values ever reported for a proton-conducting MOF,[29-31] indicating that the proton-conducting mechanism is the Grotthuss mechanism.[3] The high proton conductivity and low activation energy together manifest from adsorbing water molecules residing in suitable positions that facilitate the formation of a highly effective proton-conducting pathway. PXRD reveals that **1** can maintain its crystallinity after both water vapor adsorption and proton conduction (**Fig. 2b**).

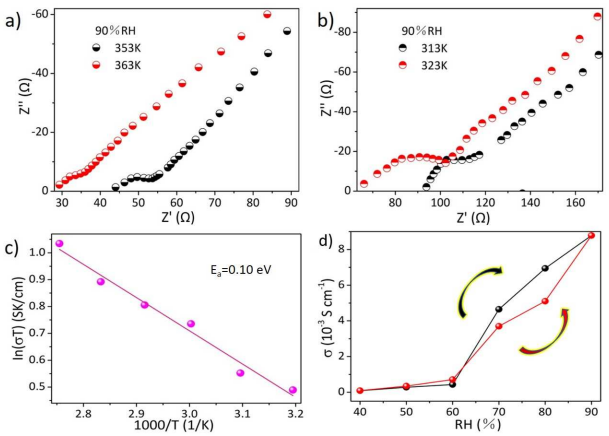

Figure 4. a) Impedance spectrum of **1** at 353 K (δ=2.21 × 10^{-2} S cm^{-1}) and 363 K (δ=2.91 × 10^{-2} S cm^{-1}) under 90% RH, and b) 313 K (δ=9.85 × 10^{-3} S cm^{-1}) and 323 K (δ=1.10 × 10^{-2} S cm^{-1}) under 90% RH. c) Arrhenius plot of the temperature-dependence on proton conductivity in **1** at 90% RH. d) Humidification (black line) and dehumidification (red line) cycles of **1** under 303 K showing nearly overlapped dependent conductivity values.

Although **1** possesses high proton conductivity exceeding 10^{-2} S cm^{-1}, surprisingly, there is no evident hydrogen-bond network existing within the structure. To confirm the pivotal role that Na^+ cations play in proton conduction, Li^+ was exchanged into **1** and identical experiments were subsequently carried out. From the ICP-MS analysis, we calculated that 33.48% of available Na^+ was replaced by Li^+, in consistency with the EDS analysis (**Table S2**). The change in proton conductivity (e.g. δ=2.52 × 10^{-3} S cm^{-1} vs. 2.91 × 10^{-2} S cm^{-1}, 363K) and activation energy (0.15 eV vs. 0.10 eV) of **1** after Li^+ exchange suggests that alkali metal cations are indeed facilitating proton conduction in this material (**Fig. S10, S11 and S12**). Therefore, a new mode of proton transportation has been revealed and is associated with the ordered Na^+ and adsorbed water in **1**. Considering both the moderate water vapor adsorption of **1** and the interaction between Na^+ and H_2O, we ensure that water molecules distribute and engulf the chain of Na^+ cations associated with terminal C=O and S=O groups as a bridging motif to conduct protons. This construct allows a highly effective proton-conducting pathway to achieve both high proton conduction and low activation energy. The proton conductivity of 2.91 × 10^{-2} S cm^{-1} of **1** is higher than most water-mediated proton-conducting MOFs[3, 32], which confirms that the one-dimensional ordered Na^+ is an essentially important motif in the process of proton transportation.

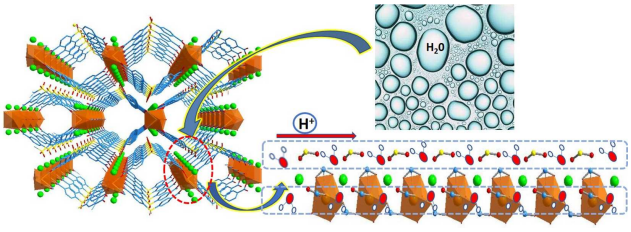

Figure 5. Mechanism of proton conduction in **1**.

In summary, we have successfully synthesized a new anionic MOF (**1**) with Na^+ ordered between pseudo-3D Eu-formate layers. Specifically, ordered Na^+ and terminal/non-coordinating oxygen atoms from nearby C=O and S=O groups cooperate to create an environment that facilitates highly effective proton conduction. Although there is no evident hydrogen-bond network in **1**, it displays both a high proton conductivity of 2.91 × 10^{-2} S cm^{-1} at 363 K and 90% RH with a low activation energy of 0.10 eV. The change in proton conductivity and activation energy of **1** after Li^+ exchange suggests that Na^+ indeed participates in the process of proton conduction and this is a new mode of proton transportation associated with ordered alkali metal cation and adsorbed water exists in **1**.

We thank the National Science Foundation of China (21790370, 21790374, 21601131), the Science Foundation of Jiangsu Province (BK20140007, BK20140303), a Project Funded by the Priority Academic Program Development of Jiangsu Higher Education Institutions (PAPD), and the "Young Thousand Talents Program" in China for financial support of this work. Support for TEA-S was provided by the Center for Actinide Science and Technology (CAST), an Energy Frontier Research Center funded by the U.S. Department of Energy, Office of Science, Basic Energy Sciences under Award Number DE-SC0016568

Conflicts of interest

There are no conflicts to declare.

Notes and references

1. T. Yamada, K. Otsubo, R. Makiura and H. Kitagawa, *Chem. Soc. Rev.*, 2013, **42**, 6655.
2. P. Ramaswamy, N. E. Wong and G. K. Shimizu, *Chem. Soc. Rev.*, 2014, **43**, 5913-5932.
3. X. Meng, H. N. Wang, S. Y. Song and H. J. Zhang, *Chem. Soc. Rev.*, 2017, **46**, 464-480.
4. A. J. Clough, J. M. Skelton, C. A. Downes, A. A. de la Rosa, J. W. Yoo, A. Walsh, B. C. Melot and S. C. Marinescu, *J. Am. Chem. Soc.*, 2017, **139**, 10863-10867.
5. C. Montoro, D. Rodriguez-San-Miguel, E. Polo, R. Escudero-Cid, M. L. Ruiz-Gonzalez, J. A. R. Navarro, P. Ocon and F. Zamora, *J. Am. Chem. Soc.*, 2017, **139**, 10079-10086.
6. B. Joarder, J. B. Lin, Z. Romero and G. K. H. Shimizu, *J. Am. Chem. Soc.*, 2017, **139**, 7176-7179.
7. S. S. Park, Y. Tulchinsky and M. Dincă, *J. Am. Chem. Soc.*, 2017, **139**, 13260-13263.
8. A. Karmakar, R. Illathvalappil, B. Anothumakkool, A. Sen, P. Samanta, A. V. Desai, S. Kurungot and S. K. Ghosh, *Angew. Chem. Int. Ed.*, 2016, **55**, 10667.
9. S. Kim, B. Joarder, J. A. Hurd, J. Zhang, K. W. Dawson, B. S. Gelfand, N. E. Wong and G. K. H. Shimizu, *J. Am. Chem. Soc.*, 2018, DOI: 10.1021/jacs.7b11364.
10. G. K. Shimizu, J. M. Taylor and S. Kim, *Science*, 2013, **341**, 354-355.
11. P. Ramaswamy, N. E. Wong, B. S. Gelfand and G. K. Shimizu, *J. Am. Chem. Soc.*, 2015, **137**, 7640-7643.
12. S. Pili, S. P. Argent, C. G. Morris, P. Rought, V. Garcia-Sakai, I. P. Silverwood, T. L. Easun, M. Li, M. R. Warren, C. A. Murray, C. C. Tang, S. Yang and M. Schroder, *J. Am. Chem. Soc.*, 2016, **138**, 6352-6355.

13. J. M. Taylor, T. Komatsu, S. Dekura, K. Otsubo, M. Takata and H. Kitagawa, *J. Am. Chem. Soc.*, 2015, **137**, 11498-11506.
14. K. Cai, F. Sun, X. Liang, C. Liu, N. Zhao, X. Zou and G. Zhu, *J. Mater. Chem. A*, 2017, **5**, 12943-12950.
15. N. T. Nguyen, H. Furukawa, F. Gandara, C. A. Trickett, H. M. Jeong, K. E. Cordova and O. M. Yaghi, *J. Am. Chem. Soc.*, 2015, **137**, 15394-15397.
16. M. Bazaga-Garcia, R. M. Colodrero, M. Papadaki, P. Garczarek, J. Zon, P. Olivera-Pastor, E. R. Losilla, L. Leon-Reina, M. A. Aranda, D. Choquesillo-Lazarte, K. D. Demadis and A. Cabeza, *J. Am. Chem. Soc.*, 2014, **136**, 5731-5739.
17. D. Gui, T. Zheng, J. Xie, Y. Cai, Y. Wang, L. Chen, J. Diwu, Z. Chai and S. Wang, *Inorg. Chem.*, 2016, **55**, 12508-12511.
18. Z. Bai, Y. Wang, W. Liu, Y. Li, J. Xie, L. Chen, D. Sheng, J. Diwu, Z. Chai and S. Wang, *Cryst. Growth Des.*, 2017, **17**, 3847-3853.
19. M. Sadakiyo, T. Yamada, K. Honda, H. Matsui and H. Kitagawa, *J. Am. Chem. Soc.*, 2014, **136**, 7701–7707.
20. A. Shigematsu, T. Yamada and H. Kitagawa, *J. Am. Chem. Soc.*, 2011, **133**, 2034-2036.
21. S. Bureekaew, S. Horike, M. Higuchi, M. Mizuno, T. Kawamura, D. Tanaka, N. Yanai and S. Kitagawa, *Nat. Mater.*, 2009, **8**, 831−836.
22. V. G. Ponomareva, K. A. Kovalenko, A. P. Chupakhin, D. N. Dybtsev, E. S. Shutova and V. P. Fedin, *J. Am. Chem. Soc.*, 2012, **134**, 15640-15643.
23. M. Sadakiyo, T. Yamada and H. Kitagawa, *J. Am. Chem. Soc.*, 2014, **136**, 13166-13169.
24. P. Bajaj, A. W. Gotz and F. Paesani, *J. Chem. Theory Comput.*, 2016, **12**, 2698-2705.
25. D. Feller, E. D. Glendening, D. E. Woon and M. W. Feyereisen, *J. Chem. Phys.*, 1995, **103**, 3526-3542.
26. M. Bazaga-García, M. Papadaki, R. M. P. Colodrero, P. Olivera-Pastor, E. R. Losilla, B. Nieto-Ortega, M. Á. G. Aranda, D. Choquesillo-Lazarte, A. Cabeza and K. D. Demadis, *Chem. Mater.*, 2015, **27**, 424-435.
27. A. L. Spek, *J. Appl. Cryst.*, 2003, **36**, 7-13.
28. Y. Wang, Z. Tao, X. Yin, J. Shu, L. Chen, D. Sheng, Z. Chai, T. E. Albrecht-Schmitt and S. Wang, *Inorg. Chem.*, 2015, **54**, 10023-10029.
29. T. N. Tu, N. Q. Phan, T. T. Vu, H. L. Nguyen, K. E. Cordova and H. Furukawa, *J. Mater. Chem. A*, 2016, **4**, 3638–3641.
30. X. Zhao, C. Y. Mao, X. H. Bu and P. Y. Feng, *Chem. Mater.*, 2014, **26**, 2492–2495.
31. S. S. Nagarkar, S. M. Unni, A. Sharma, S. Kurungot and S. K. Ghosh, *Angew. Chem. Int. Ed.*, 2014, **53**, 2638–2642.
32. C. Maxim, S. Ferlay, H. Tokoro, S. I. Ohkoshid and C. Train, *Chem. Commun.*, 2014, **50**, 5629–5632.